PLOS ONE

Nanoparticle coatings for controlled release of quercetin from an angioplasty balloon

Ioana Craciun[1], **Carlos E. Astete**[2], **Dorin Boldor**[2], **Merilyn H. Jennings**[3], **Jake D. Gorman**[2], **Cristina M. Sabliov**[2☯]*, **Tammy R. Dugas**[3☯]*

1 Department of Clinical Sciences, Faculty of Veterinary Medicine, University of Agricultural Sciences and Veterinary Medicine Cluj-Napoca, Cluj-Napoca, Romania, **2** Department of Biological and Agricultural Engineering, Louisiana State University and the LSU AgCenter, Baton Rouge, Los Angeles, United States of America, **3** Department of Comparative Biomedical Sciences, Louisiana State University School of Veterinary Medicine, Baton Rouge, Los Angeles, United States of America

☯ These authors contributed equally to this work.
* csabliov@agcenter.lsu.edu (CMS); tammydugas@lsu.edu (TRD)

Abstract

Peripheral artery disease (PAD) is a systemic vascular disease of the legs that results in a blockage of blood flow from the heart to the lower extremities. Now one of the most common causes of mortality in the U.S., the first line of therapy for PAD is to mechanically open the blockages using balloon angioplasty. Coating the balloons with antiproliferative agents can potentially reduce vessel re-narrowing, or restenosis after surgical intervention, but current drug-coated balloons releasing chemotherapy agents like paclitaxel have in some cases shown increased mortality long-term. Our aim was to design a novel drug-coated balloon using a polymeric nanodelivery system for a sustained release of polyphenols that reduce restenosis but with reduced toxicity compared to chemotherapy agents. Poly (lactic-co-glycolic acid) (PLGA) nanoparticles with entrapped quercetin, a dimethoxy quercetin (rhamnazin), as well as quercetin covalently attached to PLGA, were developed. Balloon catheters were coated with polymeric nanoparticles using an ultrasonic method, and nanoparticle characteristics, drug loading, coating uniformity and drug release were determined. The adhesion of nanoparticles to vascular smooth muscle cells and the antiproliferative effect of nano-delivered polyphenols were also assessed. Of the nanoparticle systems tested, those with covalently attached quercetin provided the most sustained release over a 6-day period. Although these particles adhered to cells to a smaller extent compared to other nanoparticle formulations, their attachment was resistant to washing. These particles also exhibited the greatest anti-proliferative effect. In addition, their attachment was not altered when the cells were grown in calcifying conditions, and in PAD tissue calcification is typically a condition that impedes drug delivery. Moreover, the ultrasonic coating method generated a uniform balloon coating. The polymeric nanoparticle system with covalently attached quercetin developed herein is thus proposed as a promising platform to reduce restenosis post-angioplasty.

Introduction

Peripheral artery disease (PAD) is a systemic atherosclerotic disease that affects approximately 202 million people worldwide. With over 8 million diagnoses, PAD is one of the most common causes of mortality in the United States [1–4]. Moreover, atherosclerotic diseases like PAD are becoming a world-wide problem [5]. PAD is characterized by debilitating atherosclerotic occlusion of arteries in the lower extremities, resulting in an obstruction of blood flow [1, 6]. Though a disease of the extremities, left untreated, PAD can culminate in catastrophic consequences like stroke, myocardial infarction, and death [2, 7]. The most common symptom among patients with PAD is intermittent claudication, but it is often asymptomatic, under-diagnosed and under-treated, resulting in a reduced functional capacity and quality of life. In its most severe form, the resulting limb ischemia can necessitate limb amputation [2–4]. To treat lower extremity PAD, clinicians often revascularize the affected artery or arteries using an endovascular procedure known as angioplasty, achieved using balloon dilation and sometimes, placement of a stent [8–11]. Angioplasty is a technique of mechanically widening a blood vessel that has been narrowed or obstructed due to atherosclerosis [12]. In PAD, balloon angioplasty is favored over stenting due to the small diameter of the affected arteries and the preponderance of stent fractures occurring in clinical cases [13, 14]. Balloon angioplasty allows slow vessel stretching to enlarge the lumen [12]. Unfortunately, it also induces stretch and strain to the vessel wall, and the injury it imparts induces a series of cellular events culminating in the formation of a new lesion [15]. Restenosis or vessel re-narrowing after implantation remains a complication of vascular interventions [16]. Early restenosis and neointimal hyperplasia within the stented vessels have been attributed to deep vascular injury, with fracture of the internal elastic lamina [17]. Intimal hyperplasia includes inflammatory phenomena, migration, and proliferation of smooth muscle cells and also, extracellular matrix deposition [17]. These events culminate in a thickened vessel wall that obstructs blood flow [15, 18].

Current protocols for the prevention and therapy of restenosis after angioplasty/stenting are based on sustained, antiproliferative drug release into the vessel wall [19]. Drug-coated balloons (DCB) have recently emerged as a treatment for peripheral artery [19–22] and coronary in-stent restenosis [23]. The concept of DCB therapy relies on healing of the vessel wall after a rapid release of drug locally but retention of the drug within the vessel wall long enough to impact deleterious cellular events occurring early after the procedure. DCBs require three fundamental elements: a semi-compliant angioplasty balloon, an antiproliferative drug and a drug carrier [23]. DCB releasing the chemotherapy agent paclitaxel have been approved by the FDA. Paclitaxel is highly lipophilic and binds quickly and tightly to tissue, which results in rapid cellular uptake and long-term retention at the site of delivery. This treatment comes with major disadvantages such as: systemic toxicity [15, 24], the release of paclitaxel before arrival at the lesion site due to direct application of drug to the balloon surface [15, 24] and delayed re-endothelialization, as demonstrated by animal studies utilizing paclitaxel-eluting stents [25, 26]. In addition, recent alerts issued by the FDA identified a late mortality signal in study subjects treated with paclitaxel-coated balloons. The relative risk for increased mortality at 5 years was 1.57 (95% confidence interval 1.16–2.13), which corresponds to a 57% relative increase in mortality in patients treated with paclitaxel-coated devices [27]. Therefore, studies focused on controlled delivery of other anti-proliferative agents have evolved. Our own prior research focused on two synergistic polyphenols—resveratrol and quercetin—and these studies demonstrated that the two have low toxicity and reduce vascular smooth muscle proliferation but promote re-endothelialization, both *in vitro* and *in vivo* [15, 28]. We were also successful in developing a drug-eluting coating that successfully achieves slow release of resveratrol (i.e.,

over several days), but by comparison, release of quercetin was more rapid and less protracted [15].

Within this framework, the aim of this study was to develop polymeric nanoparticles (pNP) for quercetin delivery that were capable of a high entrapment, slow release of drug and anti-proliferative activity. Poly (lactic-co-glycolic acid) (PLGA) nanoparticles with entrapped quercetin (pNP(eQ)), a dimethoxy quercetin (i.e., rhamnazin, designated pNP(eR)), as well as quercetin covalently attached to PLGA (pNP(cQ)), were developed. Using an ultrasonic coating method, miniaturized balloon catheters were coated with pNP, and nanoparticle characteristics, drug loading, drug release, and efficacy in reducing vascular smooth muscle cell proliferation were assessed. With respect to the coated balloons, we also determined particle deposition on the balloon surface, assessed as total pNP and drug loading, as well as coating uniformity. We aimed to achieve uniformly coated balloons, with the particles firmly adhered. Our overarching project goal is to achieve minimal loss of drug from the balloon surface during transit to the lesioned area, but upon inflation within the lesioned artery, the particles transfer and attach firmly to the vessel wall, where the coating begins releasing polyphenols. As such, we aim to achieve a controlled and localized administration of the active substance in the affected area.

A secondary aim of our design was to enable pNP adhesion to calcified lesions. Vascular calcification is a common occurrence in PAD and compared to coronary artery disease, can be extensive [29]. The accumulation of calcium and phosphate in the intimal and medial layers of the vessel are typical of patients with PAD, particularly those with chronic kidney disease and diabetes mellitus [30]. Calcification is a key contributor to poorer outcomes after angioplasty, as it leads to altered compliance, flow-limiting dissections and acute vessel recoil [31]. Moreover, late lumen loss after paclitaxel-coated balloon therapy was shown correlated with circumferential calcification [32], and hypotheses are that such outcomes are due to an inability of the calcified lesion to absorb paclitaxel. Thus, in some experiments, we tested whether our pNP coating was capable of strong adhesion to cells in which calcium accumulation was induced experimentally.

Materials and methods

Materials

The following materials were obtained from Sigma-Aldrich (St. Louis, MO): Resomer RG504H poly (D, L-lactide-co-glycolide), PLGA 50:50 (molecular weight 38,000–54,000), acetone and poly (vinyl alcohol) (PVA 31,000–50,000; 87–89% hydrolyzed), quercetin and rhamnazin. A 50:50 mole ratio of PLGA co-polymer was selected to achieve a reasonable degradation time for a drug delivery application; we expect the majority of the co-polymer will have degraded by ~4 weeks. PLGA covalently modified with quercetin was synthetized in the laboratory. Analytical grade chemicals and reagents were used for this study.

Covalent modification of PLGA with quercetin

The coupling of quercetin to PLGA was based on an acylation reaction. The first step was PLGA activation. Briefly, 2 g of PLGA was dissolved in 50 mL DCM at room temperature in a 3-neck round bottom flask. A bubbler bottle with 1 M sodium hydroxide NaOH was required to neutralize HCl produced during the reaction under nitrogen. After complete dissolution of PLGA at room temperature, 10 eq. of oxalyl chloride was added dropwise with a glass syringe, along with 3 mL of DMF. The reaction was performed at room temperature with mild stirring for 5 hours. Next, the solution was concentrated with a Buchi R-300 Rotavapor (Buchi Corporation, New Castle, DE). The activated PLGA polymer was precipitated by addition of 200–300

mL of ethyl ether. The white precipitate was washed at least three times with ethyl ether to remove impurities. The solids were dried overnight under high vacuum. The second reaction was performed by dissolution of 1 g of dry PLGA-Cl in 25 mL of DMSO, which was added dropwise to 35 mg of quercetin dissolved in 20 mL of DMSO. The reaction was performed overnight at room temperature under nitrogen. The PLGA-quercetin polymer was precipitated by addition of 150 mL of ethyl ether; the precipitation was repeated three times. The precipitated polymer was suspended in 80 mL of DCM and the organic phase was washed with 200 mL of water to remove unreacted quercetin. The process was repeated to obtain a clear supernatant. Finally, the DCM was evaporated with a Buchi R-300 Rotavapor, and the polymer was dried under high vacuum for 3 days at 30°C. The PLGA-quercetin copolymer was stored at 2–4°C for further characterization and use in nanoparticle synthesis.

Synthesis of PLGA-Eudragit RL-100 nanoparticles

The polymeric nanoparticles were synthesized employing a single emulsion evaporation technique. Briefly, an organic phase was created by mixing Eudragit RL 100 (60 mg) and PLGA (200 mg) in ethyl acetate to acetone (8:2) solution (6 mL), with mild stirring at room temperature for 30 minutes. Next, quercetin or rhamnazin was added to the organic phase. Rhamnazin was used to test whether alkylation of quercetin resulted in a protracted release profile. After 15 min and with continued stirring at room temperature, the organic phase was poured dropwise into 60 mL of aqueous phase containing 4 mg/mL Tween 80. To reduce droplet size, the emulsion was microfluidized with an M-110P Microfluidizer (Microfluidics Corp, Westwood, MA) at 4°C, 30,000 PSI, with four passes. Ethyl acetate in the suspension was evaporated using a Buchi R-300 Rotavapor (Buchi Corp., New Castle, DE) under vacuum at 32°C for 2 h. Finally, the nanoparticle suspension was mixed with trehalose at a 1:2 mass ratio, and the suspension was freeze-dried with a FreeZone 2.5 (Labconco Corp., Kansas City, MO) at 32°C for 2 days. A 2 mL solution of polyvinyl alcohol (PVA; 30 mg) was added before freeze-drying to minimize aggregation after polymeric nanoparticle resuspension. The powdered samples were kept at -80°C until further characterization and use. In some studies, PLGA was covalently modified with Q prior to pNP synthesis, but all other steps were identical. The mean size, PDI and zeta potential of the polymeric nanoparticles were measured by Dynamic Light Scattering (DLS) with a Malvern Zetasizer nano ZS (Malvern Panalytical inc, Westborough, MA). Because pilot studies demonstrated an impact of trehalose on cell growth, for studies examining the effect of nano-delivered quercetin on vascular smooth muscle cell proliferation, the pNP were prepared fresh on the day of the experiment, without freeze-drying and without trehalose. However, all other components were maintained at a similar ratio to ensure that the pNP formulations for the two studies were similar.

Nanoparticle characterization

Morphology. Transmission electron microscopy (TEM) was accomplished using a JEOL JM-1400 (JEOL USA Inc., Peabody, MA) and an accelerating voltage of 120 kV. As such, TEM was used to analyze the structure of empty PLGA polymeric nanoparticles (pNP(E)), PLGA NP with entrapped rhamnazin (pNP(eR)), PLGA pNP with entrapped quercetin (pNP(eQ)) and PLGA NP with covalently attached quercetin (pNP(cQ)). One drop of the pNP resuspension in nanopure water was placed onto a carbon film 400 mesh copper grid, and the excess amount of solution was removed with sterile filter paper. A solution of 2% uranyl acetate was used for staining. After 5 min, a separate sterile filter paper was utilized to remove excess uranyl acetate.

Size distribution and zeta potential characterization.   Dynamic light scattering (DLS) (Malvern Panalytical, Westborough, MA) was employed to characterize the nanoparticles for size, polydispersity and zeta potential. After resuspension in low resistivity water, a disposable capillary cell of 1 mL volume was used to measure size, polydispersity index (PDI), and zeta potential (Smoluchowski model) for NP.

Drug release and biologic efficacy

Drug release protocol.   The release profiles were performed by placing 10mg/mL PLGA-Eudragit RL100 NP (pNP(eQ), pNP(eR), pNP(cQ)) in dialysis membrane (molecular weight cut-off of 12,000/14,000 g/mol, regenerated cellulose, Fisher Scientific). Sterile PBS was used for sample resuspension. The samples were dialyzed against 800 mL of PBS at 37°C under continuous stirring, and PBS was replaced every 8 h in the first 12h and then every 24h. At pre-determined time points, 0.2 mL samples were taken from inside the dialysis bag (nano-particle solution) and to prevent quercetin oxidation, was mixed with 20 μL of 50 mM ascorbic acid. Finally, 800 μL of DMF was added to extract the active components. The samples were vortexed for 1h at room temperature and then stored at -80°C until drug concentrations could be measured using a high-performance liquid chromatography (HPLC) method we described previously [15].

Cytotoxicity and cell proliferation assay.   Rat aortic smooth muscle cells (RAOSMC; Cell Applications, Inc., San Diego, CA) were grown to confluency in 96-well culture plates using low-glucose DMEM growth medium containing 10% Fetal Bovine Serum (FBS) and 1% anti-mycotic/antibiotic (penicillin-streptomycin/amphotericin B). To simulate a brief balloon infla-tion and delivery of pNPs, the cells were incubated at 37°C for 2 hours in low-glucose DMEM containing DMEM 2% FBS and 0–1.4 mg/mL of either empty pNP (pNP(E)), or quercetin-containing pNP, including pNP(eQ), pNP(eR) or pNP(cQ). We selected 2 hours because pilot observations determined that 2 hours was the minimum amount of time required for pNP to fall to the bottom of the well and adhere. Drug-containing medium was removed and the cells were washed with 100 μL PBS and then incubated with DMEM grown medium. Cytotoxicity was assessed at 24, 48 and 72 h using the CellTiter-Glo® Luminescent Cell Viability Assay (Promega). Essentially, the assay determines the level of ATP present in the cells, indicative of metabolically activity.

To test whether quercetin-containing pNPs could impact restenosis after a brief balloon inflation, RAOSMC were grown to 50–60% confluence in 24-well plates containing low-glu-cose DMEM growth medium. To synchronize cell cycle, the grown medium was removed and replaced with DMEM containing 0.1% FBS. After serum-starvation for 72 h, cell proliferation was stimulated using low-glucose DMEM containing 10% FBS and 0–0.4 mg/mL of either empty pNP (pNP(E)), or quercetin-containing pNP, including pNP(eQ), pNP(eR) or pNP (cQ). Cell proliferation was assessed by following the rate of DNA synthesis, determined as the amount of 5-bromo-2′-deoxy-uridine (BrdU) incorporation (Roche BrDU Labeling and Detection Kit II, Sigma-Aldrich, St. Louis, MO). Briefly, 100 μL BrdU labelling reagent was added to each well and the plates were incubated for 2 h at 37 °C. The medium was aspirated, 300 μL Fixdenat was added, and the plates were incubated for 30 min at room temperature. Next, the Fixdenat was aspirated and 300 μL peroxidase conjugated anti-BrdU antibody was added to all wells, including the background control wells, and the plates were incubated for 90 min at room temperature. The wells were then washed 3 times with 300 μL washing buffer, and 300 μL of substrate were added and allowed to incubate for 2 minutes in dark conditions and at room temperature. Finally, 75 μL 1M H_2SO_4 were added to each well, and after rotating for 2 minutes, absorbance was read at 450 nm (reference 690 nm) using a Biotek Synergy

microplate reader. Data were expressed as a percent of control cells stimulated with only 10% FBS but with no nanoparticles.

Adhesion study protocol. Because endothelial cells are denuded during angioplasty, smooth muscle cells are the predominate cell type exposed to the balloon to accept pNP containing polyphenols during balloon inflation. Moreover, as explained in the introduction, these cells are typically calcium-laden in PAD. Thus, to model advanced calcified lesion in PAD, RAOSMC were cultured and maintained in a black-walled, clear bottom, tissue-culture treated plates with growth medium compared to calcification medium for two weeks [33]. Growth medium contained DMEM with 10% fetal calf serum. Calcification medium contained high glucose (4.5 g/L) DMEM with 10% fetal calf serum, 100 U/mL penicillin, 100 μg/mL streptomycin, 6 mmol/L $CaCl_2$, 10 mmol/L sodium pyruvate, $10-6$ mol/L insulin, 50 μg/mL ascorbic acid, 10 mmol/L β-glycerophosphate and $10-7$ mol/L dexamethasone. Calcification was confirmed using Von Kossa staining (S1 Fig). Next, 10 mg/mL suspensions of pNP(E), pNP(eQ), and pNP(cQ) were diluted in PBS to a final concentration of 2.0 mg/mL. From each suspension 100 μL were placed in wells of the culture plates containing calcified/uncalcified RAOSMC and the cells were incubated at 37˚C for 2 hours. We selected 2 hours because pilot observations determined that 2 hours was the minimum amount of time required for pNP to fall to the bottom of the well and adhere. Drug-containing medium was then removed and the cells were subjected to a 100 μL PBS wash before every well was aspirated to dryness. Fluorescence intensity was quantified before and after washing using a Biotek Synergy 2 fluorescence plate reader. Measures of fluorescence detected for cells containing no pNP were used for background correction. In addition, after washing, green fluorescence images of wells were captured on a ZOE Fluorescent Cell Imager (Bio-Rad, Hercules, CA). Lysis buffer was then placed in wells so that protein levels could be quantified by BCA protein assay. Measures of fluorescence units were normalized to μg protein in each well. Original fluorescence images collected using the ZOE Fluorescent Cell Imager are available in the Open Science Framework (OSF) repository at https://osf.io/2p4ar/?view_only=f74778d5a7a34aef9f209e9c6c578b8d.

Balloon coating and characterization

Balloon fabrication, ultrasonic coating and coating morphology. A balloon catheter with a 13.8 cm extrusion, a 2.7 FR polycarbonate luer fitting and a 1.25 mm x 10 mm PET over-the-wire balloon was custom manufactured by Interplex Medical, LLC (Milford, OH). Eight balloons were shipped directly to Sono-Tek Corporation (Milton, NY), where they were professionally coated with pNP(eQ) using the following ultrasonic coating method. First, the sample for coating was drawn into a 10 mL syringe, was affixed to a MediCoat BCC coating system and was allowed to reach room temperature. Prior to coating, an atomization test was conducted using a Sono-Tek 48 kHz Accumist nozzle. The material was found to coat flawlessly at low power output. A 3-axis XYZ Gantry System (500 mm x 500 mm x 100 mm), a rotator and the appropriate mounting hardware was interfaced to the system to accommodate the balloon catheter. The balloons were inflated and coated using 5, 10, 15 or 20 layers with n = 2 balloons coated per group, so that the impact of deposition amount on uniformity and drug loading could be determined. Note that the prohibitive costs of the balloon catheters precluded our ability to test more than 8 balloons.

To obtain a gross assessment of coating morphology, scanning electron microscopy (SEM) was conducted using a Quanta 3D FEG dual beam electron microscope. Under a microscope, one over-the-wire balloon coated with 20 layers of pNP was dissected from the catheter using a scalpel. Conducted carefully so as not to disrupt the coating, 3 small sections of the balloon were removed and were mounted on an SEM stab using double-sided carbon-coated tape. The

SEM voltage was set at 5kV and images were obtain at magnifications ranging from 1000 to 40,000x.

Fluorescence imaging to quantify pNP loading and uniformity of coating. The balloons were affixed on microscopic slides with tape, making every effort to keep them aligned with the center of the slide (deviation of $\leq 3°$). Microscopic images were acquired at 4x magnification using a Cytation 3 Image reader (BioTek Instruments Inc, Winooski, VT) in TIFF format, with a 16-bit resolution, both in the visible range and in fluorescent mode. In order to image the entire balloon in a single sequence, the field of view was panned in sequential images, and 7–9 images (corresponding to individual adjacent sections of each balloon) were captured for each balloon. In one case the balloon exceeded the image edges at 4x magnification, so a "top" and a "bottom" image were later combined using the Stitching [34] plugin provided by Fiji (formerly *ImageJ*) analysis software. The images were acquired with the same imaging parameters (LED intensity = 3, integration time = 100 ms, camera gain = 14), preselected based on the "best" image obtained for a 20 layer-coated balloon, to avoid overly saturating the image brightness of the samples with thinner coatings. As will be apparent in Results, images of one 20 layer-coated balloon (20LYR1) were slightly over-saturated toward the edges of the balloon. However, this did not impact the resulting quantitative measures, as these measurements were performed mainly along the center axis of the balloon. The fluorescent loadings were quantified based on the histograms of two rectangular regions of interest (ROI) per image (Fig 1), each of them 100,000 (500x200) pixels in size (total of 12–14 histograms per coated balloon sample; see the Excel file in OSF repository for the exact number of images and histograms for each balloon sample) corresponding to 540,832 μm^2 (0.54 mm^2). The pixel size calibration was
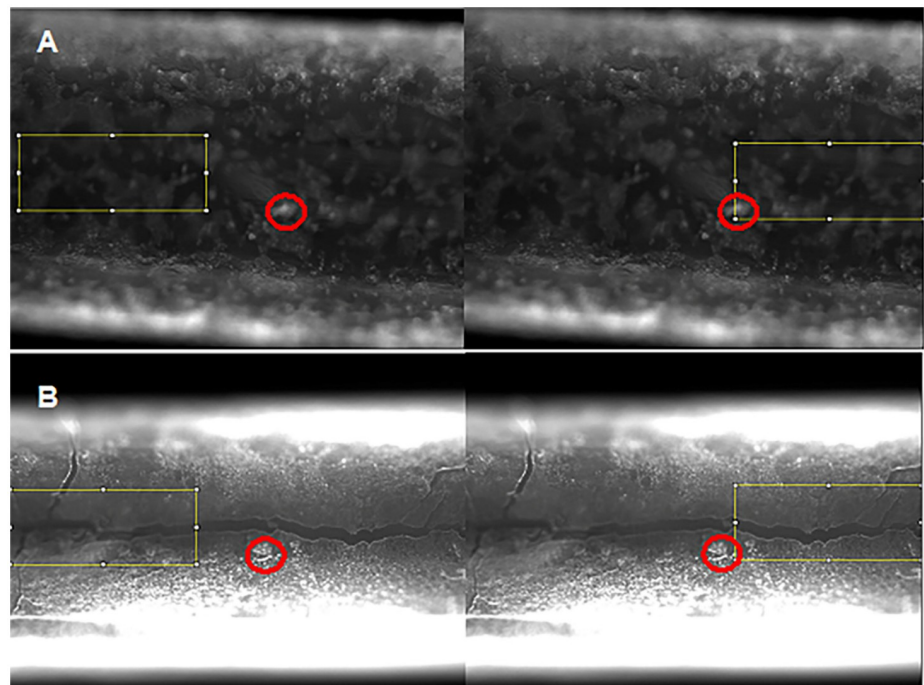

Fig 1. Representative balloon coating images illustrating methods used for assessing uniformity. Red circles indicate points of reference for recording the location of segments examined (yellow boxes). Each picture has a width of 1973 μm and a height of 1457 μm, and the illustration highlights two distinct areas (left-right) for histogram-based fluorescence analysis. In **A (top row),** balloon 1 coated with 5 layers (5LYR1), the red circle is 5941 μm from proximal end, and in **B (bottom row),** balloon 2 coated with 15 layers (15LYR2), the red circle is 5504 μm from the proximal end.

https://doi.org/10.1371/journal.pone.0268307.g001

performed using a separately acquired images at the same parameters that included a 400 μm scale bar, corresponding to 172 pixels. Note that although the instrument did not automatically save scale bars for each image, an image file used for scale analysis is included in the OSF repository. The ROIs were located along the longitudinal axis as identified using equal distances from the top and bottom edges (all histogram locations and data is available in the Excel file in the public repository). The quantification was performed by measuring the mean intensity in each ROI, then averaging the means across all ROIs for a given balloon. Additionally, the overall fluorescence was determined by integrating all brightness values in each histogram and averaging the total brightness across all ROIs for a given balloon. Coating uniformity was determined based on two separate measurements:

1. The first measurement used the standard deviation of each histogram, with higher standard deviations indicating a less uniform distribution. However, as the images were much "brighter" for the balloons containing higher loading, these values may not be used very reliably to compare balloons possessing differing numbers of layers; i.e. the balloons with fewer layers (thus lower intensities overall) will always have smaller standard deviations compared to the balloons with more layers and larger overall brightness.

2. As an alternative for uniformity of distribution, we also quantified the percent of each histogram area that had brightness intensity within ± 1-SD, which is likely a better indicator of uniformity of distribution, as it indicates how many pixels (or μm^2) have a brightness of Mean ±SD.

All image analyses were performed using Fiji software, and corresponding histogram data was exported into Excel for analysis before plotting using GraphPad Prism version 9 Software (La Jolla, CA). The quantitative data and all original images are provided in an archived OSF repository.

Quantification of pNP and drug loading using gravimetric analysis and HPLC

Prior to gravimetric analysis, the balloons were clipped from their catheters and were dried under vacuum for 1 hour. Their weights were measured using a Radwag analytical balance. The coating was then eluted using a 1:1 mixture of 90% acetonitrile: dimethylformamide. The coating suspension was acidified with ascorbic acid, vortexed vigorously and centrifuged. The supernatants were stored at -80˚C until HPLC analysis. Finally, the balloons were dried again under vacuum and weighed, so that total coating weights for each balloon could be determined.

Statistics

All data in the figures are expressed as means ± SD. For most of the biologic studies, experiments were designed to compare effects of both dose and pNP types. Thus, data were analyzed using two-way ANOVA with Bonferroni's posthoc tests using GraphPad Prism software (San Diego, CA). The exception is that for the experiments aimed at testing cell adhesion in calcifying growth conditions, three conditions were compared: calcification, washing and pNP treatment. Thus, in this case, a three-way ANOVA (with Bonferroni's posthoc tests) was conducted.
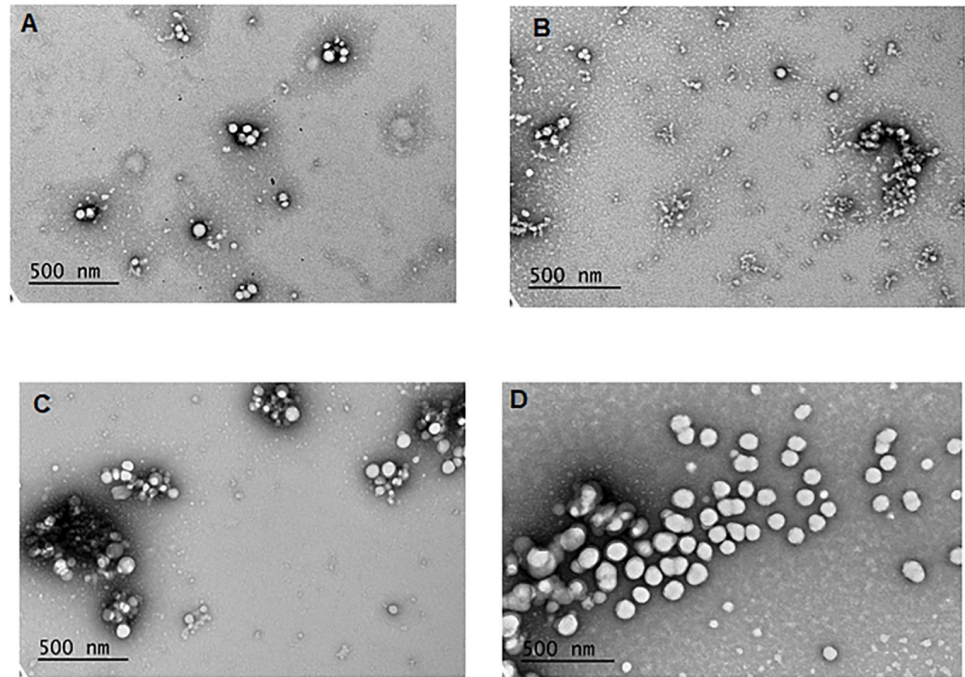
Fig 2. TEM images of (A) empty pNP (pNP(E)); (B) pNP with entrapped rhamnazin (pNP(eR)) at magnification of 50,000X; (C) pNP with entrapped quercetin (pNP(eQ)); and (D) pNP with covalently attached quercetin (pNP (cQ)) at magnification of 80,000X.

https://doi.org/10.1371/journal.pone.0268307.g002

Results and discussion

Nanoparticle characterization

Empty pNP, pNP with entrapped quercetin, pNP with entrapped rhamnazin, and pNP with quercetin covalently attached to PLGA were spherical in shape with a narrow size distribution (Fig 2 and Table 1). The particles ranged in size from 64.9 ± 0.8 nm to 161.9 ± 26.6 nm and were monodispersed (polydispersity index (PDI) < 0.2). The exception was rhamnazin entrapped pNP, which exhibited a PDI of 0.34 ± 0.016 (Table 1). Empty pNP and pNP loaded with polyphenols quercetin and rhamnazin possessed a small positive charge, with zeta potentials of +6.4–9.3 mV, while pNPs with covalently attached quercetin possessed a negative charge (zeta potential = -29.9 ± 2.4 mV; Table 1).

Drug release study

The drug release profile for all 3 entrapped active substances was measured over 6 days. The formulations with entrapped drugs exhibited a burst release within the first day, followed by a

Table 1. Physical Characteristics of the nanodelivery systems.

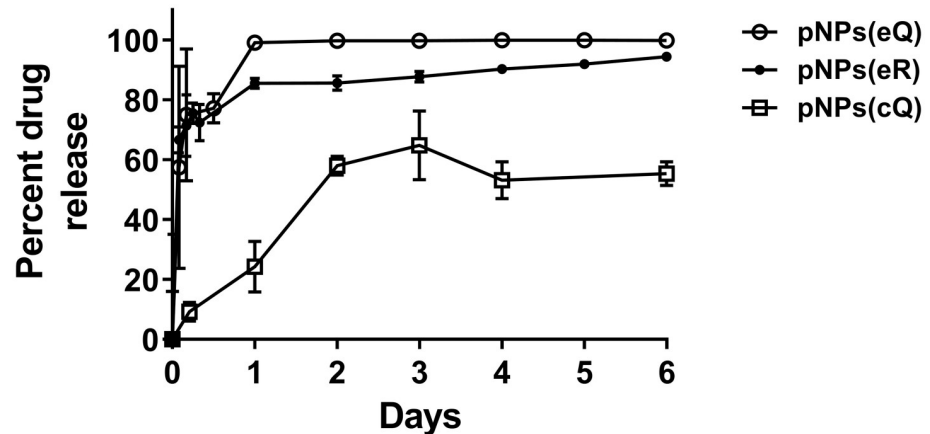|	Size (nm)	PDI	Zeta potential (mV)
Empty nanoparticles	64.9 ± 0.8	0.129 ± 0.032	6.4 ± 0.3
Entrapped quercetin pNPs	67.3 ± 1.0	0.169 ± 0.003	5.9 ± 0.6
Entrapped rhamnazin pNPs	161.9 ± 26.6	0.342 ± 0.016	9.3 ± 0.4
pNP with covalently attached quercetin	106.6 ± 0.8	0.050 ± 0.03	-29.9 ± 2.4

https://doi.org/10.1371/journal.pone.0268307.t001

Fig 3. Measures of percent drug release from pNP containing entrapped quercetin (pNP(eQ)), covalently attached quercetin (pNP(cQ)) and entrapped rhamnazin (pNP(cR)). Protracted release was observed mainly for pNPs(cQ). Data are means ± SD for n = 3.

https://doi.org/10.1371/journal.pone.0268307.g003

more gradual drug release over the remainder of the 6-day period. While entrapped quercetin released rapidly, with 99.7% of the pNP-entrapped quercetin released by day 3, the release was slightly delayed when more hydrophobic alkylated quercetin (rhamnazin) was used, with 87.7% released by day 3. The covalent attachment of quercetin to PLGA further delayed its release, as indicated by no burst release, only 64.8% release by day 3, and a gradual release over the remaining 3 days of incubation (Fig 3).

Cytotoxicity and cell proliferation assays

Prior to determining cell proliferation, maximum tolerated concentrations of polyphenol-containing pNPs were determined. To assess pNP toxicity, cells were grown to confluence, subjected to a brief pNP exposure. After washing, cell viability was assessed at 24–72 hours using by determining relative ATP levels. Although the particles were generally well tolerated by the cells, there was a mild ~20% reduction in ATP levels at the 24-h timepoint for cells treated with concentrations greater than 0.8 mg/mL of pNPs(E), pNPs(eR) and pNPs(eQ) (Fig 4). These reductions in ATP levels resolved by 48–72 h. By 72 h, some cells exhibited ATP levels greater than that of control wells. Cells treated with pNPs(cQ) demonstrated very little toxicity, with the 0.8 mg/mL dose eliciting a 20% reduction in ATP levels at 0.8 mg/mL (p<0.05) and at 24h only but exhibiting no reduction at higher doses and at no other time points. Although a mild cytotoxicity was suggested for some doses, these levels are likely an order of magnitude above what might be expected for their use *in vivo*.

For assessing cell proliferation, 0.4 mg/mL pNPs was selected as a concentration that exhibited no cytotoxicity in the cell viability assay (Fig 4). In brief, RAOSMC were synchronized, stimulated with 10% FBS ± 0.4 mg/mL empty or drug-loaded pNP for 2 h and rates of cell proliferation were assessed at 24, 48, and 72 hours as relative rates of BrDU incorporation. These relative rates are expressed as a percent of BrDU incorporation assessed for controls cells receiving no treatment. A two-way ANOVA revealed a significant effect of treatment, time and a significant interaction between treatment and time (Fig 5), with all pNP treatments significantly reducing RAOSMC proliferation by 11 to 30% at 24 hours. Note that at this initial time point, even empty pNP—pNP(E)—reduced cell proliferation, though the greatest effect was observed for entrapped quercetin (pNP(eQ)). By 48 hours, however, only the drug-containing particles significantly reduced proliferation and by 72 hours, only pNP covalently modified with Q—
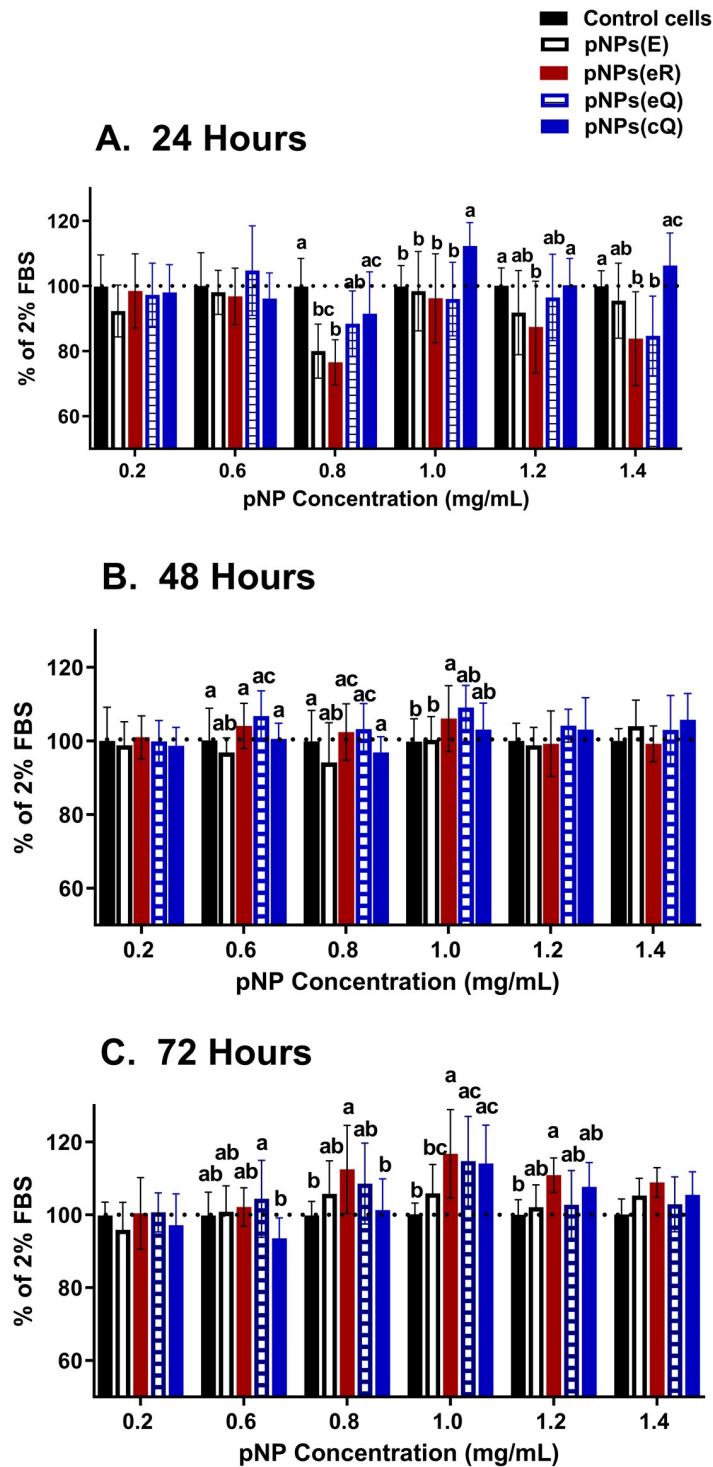
Fig 4. Rat aortic smooth muscle cells loaded for 2 hours with empty pNPs (pNPs(E)), entrapped quercetin (pNPs (eQ)), covalent quercetin (pNPs(cQ)) and entrapped rhamnazin (pNPs(eR)) exhibit only mild cytotoxicity at A) 24, B) 48 and C) 72 hours. Cytotoxicity, assessed as relative ATP levels using a luminescent assay, was compared to control cells treated with no pNPs. Data are means ± SD for n = 12. Two-way ANOVA revealed a significant effect of treatment. Means denoted by unlike letters represent significant differences for the same dose, revealed using Bonferroni's post-hoc tests.

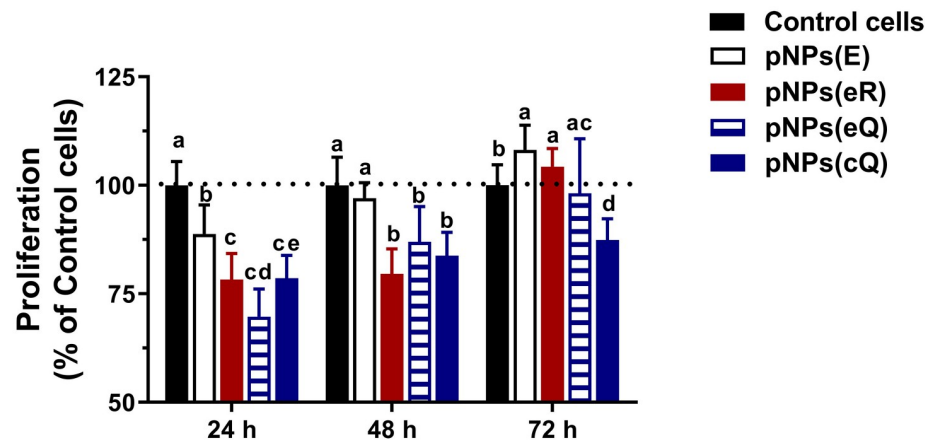https://doi.org/10.1371/journal.pone.0268307.g004

Fig 5. Rat aortic smooth muscle cells loaded for 2 hours with empty pNPs (pNPs(E)), entrapped quercetin (pNPs(eQ)), covalent quercetin (pNPs(cQ)) and entrapped rhamnazin (pNPs(eR)) exhibit reduced rates of cell proliferation at 24, 48 and 72 hours after washing. Cell proliferation was assessed by determining the incorporation of BrDU compared to control cells treated with no pNPs. Data are means ± SD for n = 8. Two-way ANOVA revealed a significant effect of treatment. Means denoted by unlike letters represent significant differences for the same time point, revealed using Bonferroni's post-hoc tests. Dotted line represents the response for control cells treated with no pNPs, denoted as 100%.

pNP(cQ)—maintained its inhibitory effect. Of note, by 72 hours, the empty pNPs exhibited a significant increase in RAOSMC proliferation, although it is unclear whether the 8% increase in proliferation observed for this treatment group and time point is of biologic significance.

Measures of pNP adhesion

Zeta potential measures showed that the pNP(cQ) possess a negative, rather than a positive charge. Thus, we hypothesized that upon balloon inflation, these particles would exhibit a reduced ability to bind the negatively charged phospholipid bilayer. However, typically, atherosclerotic arteries in PAD are calcified, with tissues accumulating calcium hydroxyapatite. Calcium hydroxyapatite crystals contain both positive and negative ions and its surface charge is highly dependent upon pH [35] Thus, we further hypothesized that given the ionic nature of calcium hydroxyapatite crystals, the pNP may actually exhibit considerable binding to smooth muscle that has become calcified. To test this hypothesis, we allowed the pNP to adhere to RAOSMCs, with one cohort of these cells cultured under calcification conditions. We used fluorescence imaging to quantify pNP adhesion given the ability of quercetin to fluoresce strongly. Results were that pNP containing Q, including eQ and cQ, exhibited greater fluorescence compared to pNP containing no Q (pNP(E); Figs 6 and 7). Fluorescence imaging generally supported this finding, except that we noted for cells treated with pNP containing covalently attached quercetin, strong fluorescence was detected in clusters among cells that were calcified (Fig 8). We theorize that perhaps these clusters represent pNP(cQ) binding to calcium hydroxyapatite crystals within the smooth muscle cell cultures. A limitation of our findings is that our assay may not preclude the possibility that the cells phagocytosed the pNPs during the 2 h incubation period. Nevertheless, pilot studies had determined that 2 h were required for the pNPs to sink to the bottom of the wells, so we anticipate that the level of phagocytosis should be small at this time point.

Loading based on fluorescence and the uniformity of coating distribution

As a gross assessment of pNP coating morphology, SEM images were captured in small sections of over-the-wire balloon that were carefully excised and flattened for imaging. As shown
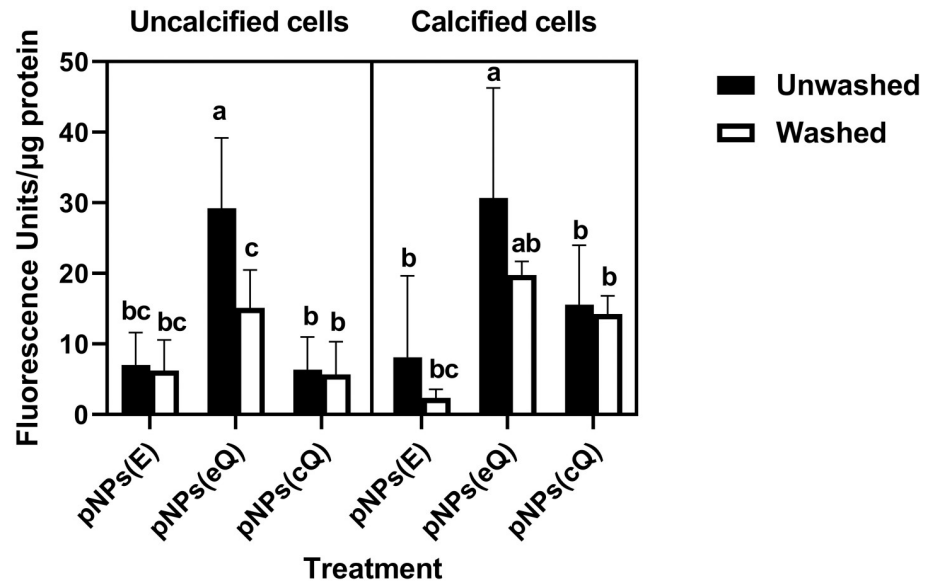
Fig 6. pNPs(cQ) exhibit a reduced ability to bind to rat aortic smooth muscle cells but their binding is resistant to washing and calcification. pNP suspensions at 2 mg/mL were allowed to bind to cells for 2 hours before washing with buffer. Some sets of cells were subjected to a calcification treatment prior to pNP exposure. Green fluorescence determined before and after washing was normalized to protein in the well. Data are means ± SD for n = 9. Three-way ANOVA revealed a significant effect of pNP treatment, calcification and washing. Means denoted by unlike letters represent significant differences for the same cell growth conditions, revealed using Bonferroni's post-hoc tests.

in Fig 9, the pNP coating generated a 3-dimensional nanostructured topography, which was particularly visible at 3000–10,000x.

The results of the fluorescence image analysis indicate that increasing the number of layers increased the fluorescence intensity of the coating, as expected. Note that balloons were named by denoting 1) the number of layers applied (i.e., 5 layers = 5LYR), followed by 2) balloon sample number (e.g., 5LYR2 = balloon sample 2 coated with 5 layers). For illustration purposes, the fluorescence and brightfield images were stitched together to reconstruct the whole balloon [34], and overlayed (Fig 10A–10D). There was a clear difference between the samples with 5 layers (5LYR1 and 5LYR2) and the ones with 20 layers (20LYR1 and 20LYR2) (Fig 10E). However, for balloons with an intermediate number of layers (10LYR1-15LYR1), differences in mean brightness were not clearly distinct from one another, even though both of these had a clearly decreased brightness compared to those with 20 layers, and an increased brightness compared to those with 5-layer balloons. These findings are supported by the drug loading data presented in Fig 11, where the balloons with 10 and 15 layers show relatively similar amounts of quercetin loadings. These findings may not necessarily indicate an issue with the coating process, as 10LYR2 and 15LYR2 were found to have good coating uniformity across the balloon surface as indicated by both the standard deviations and percent coverage. Overall fluorescence as determined by integrating brightness values over the whole ROIs yielded similar results as the mean values and thus, are not presented here. Original images (both visible and fluorescent) for all balloon sections are provided in the OSF file repository).

Standard deviations for the histograms (Fig 10E) suggest that the uniformity of coating deposition decreases with an increasing number of layers deposited. However, these findings may be biased by the fact that balloons with fewer coating layers would have much lower overall brightness and thus, smaller standard deviations associated with those mean values. To compensate for differences in standard deviations due to differences in the magnitude of
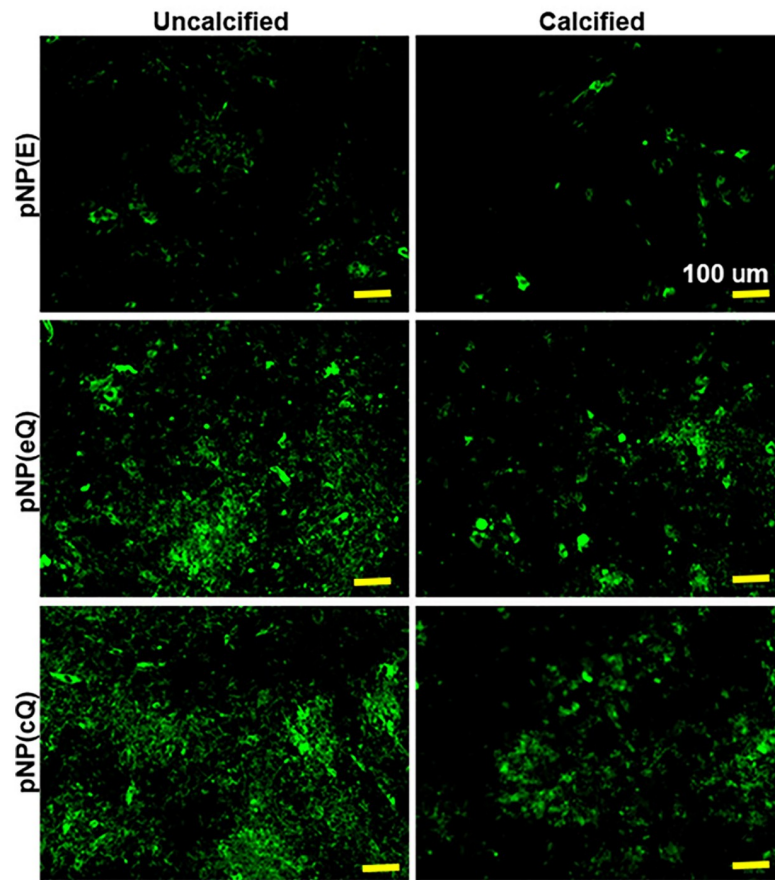
Fig 7. Representative images of green fluorescence within rat aortic smooth muscle cells exposed to pNPs containing quercetin. pNP suspensions at 2 mg/mL were allowed to bind to cells for two hours before washing with buffer. Some sets of cells were subjected to a calcification treatment prior to pNP exposure (right panel). Green fluorescence was imaged after washing. Yellow bar = 100 μm. For better visibility, yellow bars were added as an overlay to automatically saved scale bars.

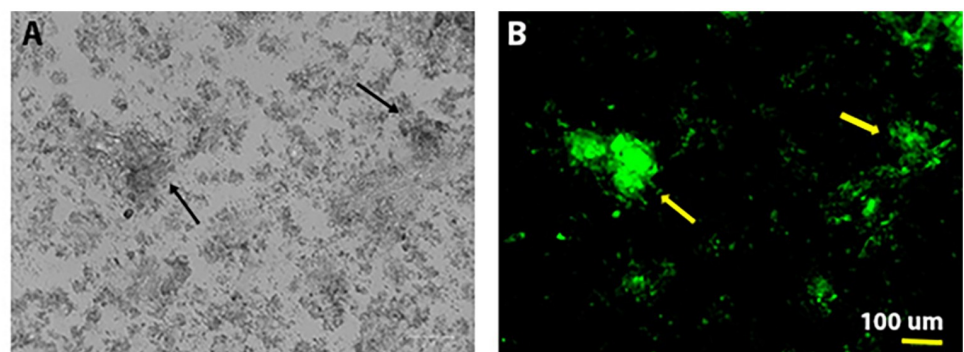https://doi.org/10.1371/journal.pone.0268307.g007

Fig 8. pNPs containing covalently attached quercetin exhibit binding to clusters (indicated by arrows) within calcified smooth muscle cell cultures that were visible in both brightfield (A) and fluorescence (B) images.
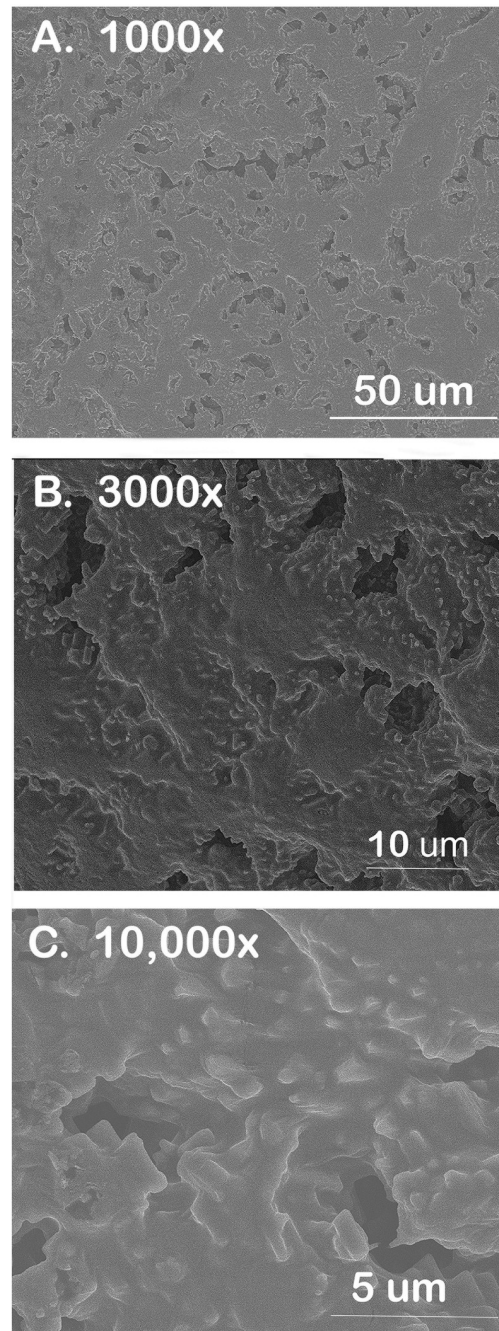
https://doi.org/10.1371/journal.pone.0268307.g008

Fig 9. Scanning electron microscopy (SEM) identifying nanostructured topography of pNPs coated onto an over-the-wire balloon. Segments of the balloon were carefully dissected from the balloon catheter under a light microscope before transferring to an SEM stab for imaging. Shown are representative images acquired at A) 1000x, B) 3000x and C) 10,000x magnification.

https://doi.org/10.1371/journal.pone.0268307.g009

overall brightness, standard deviations were normalized to the mean of each histogram (Table 2). This additional analysis indicates that two of the balloons (10LYR1 and 15LYR1) exhibited a deviation of more than 25% of the mean value, which may be indicative of a lower uniformity of coating compared to the other samples.
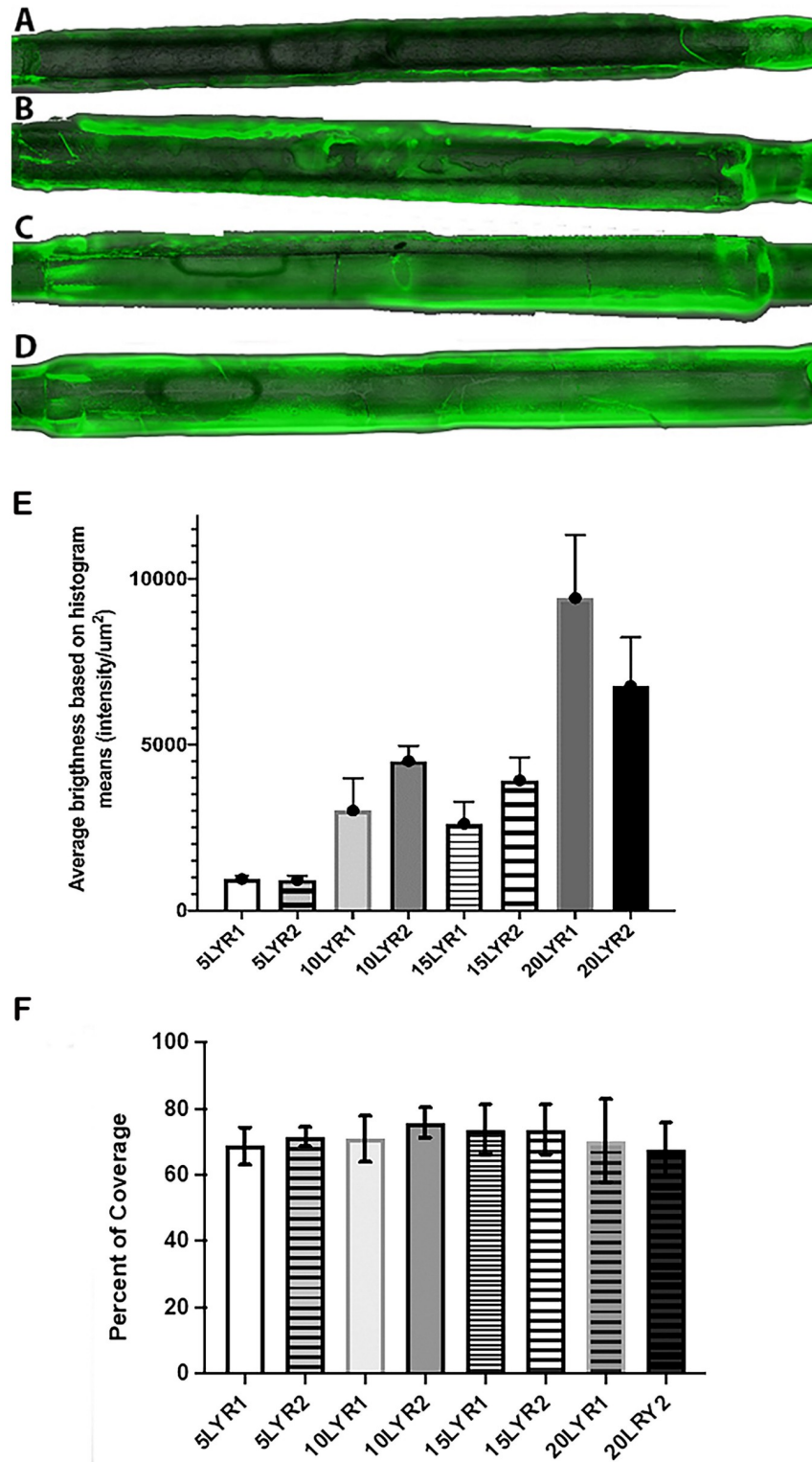
Fig 10. Fluorescence imaging revealed that ultrasonic coating with pNPs entrapping polyphenols yields uniform coatings. A) Example of stitched images used to reconstruct the balloons for image analysis. Shown are representative balloons coated with 5 (A), 10 (B), 15 (C), and 20 layers (D) of pNp coating, visible + fluorescent green overlay (at 75% opacity). E) Overall mean fluorescence and corresponding standard deviations for n = 8 samples (balloons ultrasonically coated). Data illustrated in the graph represent mean fluorescence ± SD (in unit of brightness per μm^2).

Maximum brightness for a 16-bit image is 65535, corresponding to 12117.42 per μm^2. B) Percent of balloon area that has pixels with fluorescence intensity within a ± 1-SD of the mean fluorescence. Data represent means ± SD for n = 8 samples. Higher value indicates better uniformity.

The second histogram-based measurement of coating uniformity was determined by quantifying the percent area in each histogram that has pixels with brightness (*i.e.* fluorescence) within ± 1-SD of the mean value. This measurement should be independent of absolute pixel brightness in a given ROI. Thus, this value can be used more reliably to compare uniformity between samples with differing numbers of layers (Fig 10F). Based on these measurements, the percent area covered ranged from 67.6 to 75.8%, which can be considered from good to excellent coverage or uniformity, based on a uniformity scale of: <55% poor, 55–60% moderate, 60–70% good, 70–75% very good, 75–80% excellent, >80% outstanding, with outstanding
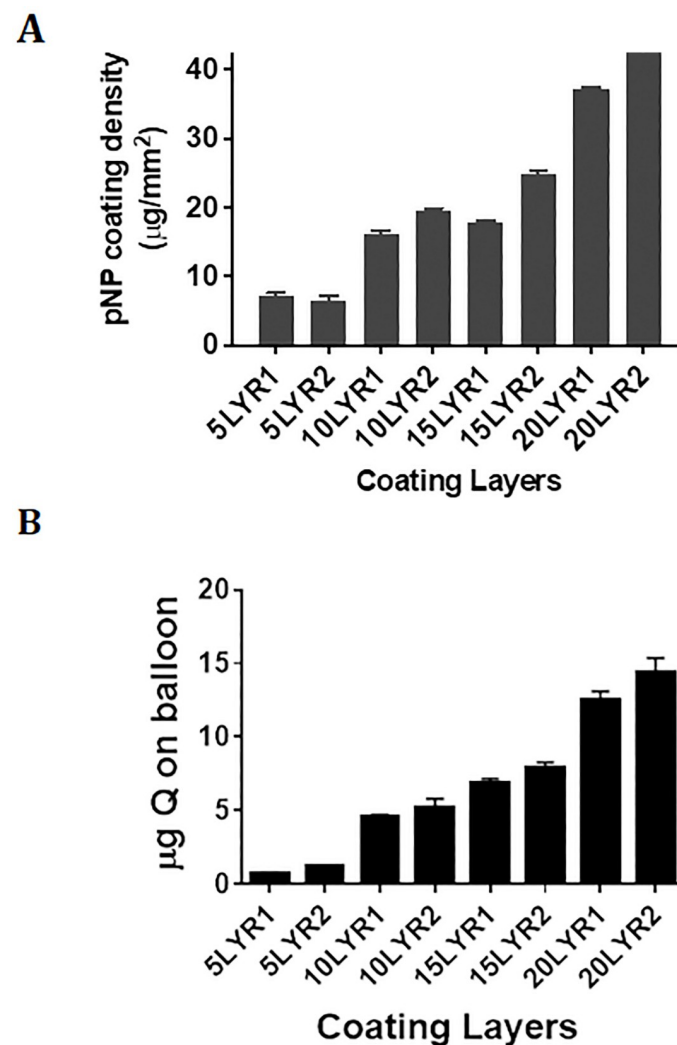
Fig 11. Amount of quercetin (Q) and quercetin nanoparticles (pNPs) in balloon coating. A) pNPs were eluted from the balloons using organic solvent and pNP load was determined gravimetrically. Total loading in μg was normalized to balloon areas. Data represent means ± SD for 5 measures per balloon. B) pNPs were eluted from the balloons using organic solvent and the Q content was determined using HPLC. Data represent means ± SD for n = 3–4 replicate measures/balloon.

Table 2. Average fluorescence brightness, absolute standard deviations, and normalized standard deviations for the coated balloons (max possible brightness = 12117.4/μm^2).

	Average brightness (intensity/μm^2)	Absolute STD (intensity/μm^2)	Normalized STD (% of mean)
5LYR1	955.38	108.16	11.3%
5LYR2	908.64	137.25	15.1%
10LYR1	3029.37	975.13	32.2%
10LYR2	4502.90	458.34	10.2%
15LYR1	2547.79	661.59	26.0%
15LYR2	3919.94	694.69	17.7%
20LYR1	9422.61	1905.54	20.2%
20LYR2	6787.45	1467.44	21.6%

https://doi.org/10.1371/journal.pone.0268307.t002

very rarely occurring in normal image processing of spray-type coatings (a 100% value would indicate all pixels in the ROI having the exact same value, which would be nearly impossible to achieve).

Several of the balloon samples showed cracking of the fluorescent coating layers (but not of the balloons themselves), clearly visible in the fluorescent images which may have an unquantified influence on the results of the image analysis, but based on the visual inspection of the images, these were relatively sparse and otherwise small overall. As the coating process occurred in a different location than the fixation on the slide and subsequent imaging, it cannot be ascertained if the cracks are a result of the coating process itself or an artifact introduced by the maybe too rapid drying after coating, or by handling during transport and slide fixation. The uncertainties introduced by these variables (different locations between coating and analysis, handling and balloon manipulations, etc) do not allow a definitive identification of the causes leading to cracking. As the samples with the smallest number of layers (5LYR1 and 5LYR2) did not exhibit any visible cracking, it seems that this phenomenon occurs only for thick layers, which, upon drying, may be more prone to cracking. As a necessary component of our coating development, further studies are needed to investigate this particular phenomenon. Additional formulations with plasticizer compounds (that decrease the brittleness of the coating upon drying) would need to be investigated if the cracking phenomenon turns out to be an impediment in the clinical deployment of these tools.

Loading of pNP and quercetin, assessed using gravimetric analysis coupled to HPLC

Gravimetric analysis mirrored the results of the fluorescence analyses. pNP coating weights increased nearly linearly with increasing numbers of layers, although coatings with 10 and 15 layers contained more similar amounts of deposited pNP compared to other groups (Fig 11A). In total, 0.26–1.5 mg of pNP were successfully applied through 5–20 coating layers, respectively (not shown). Adjusting for the surface area of the balloon, this amounted to 7–40 μg/mm^2 (Fig 11A). HPLC analysis of pNP eluted from the balloons revealed a more linear increase in quercetin levels as the coating layers were increased, with total quercetin loading ranging from 0.8–14 μg through 5–20 layers, respectively (Fig 11B).

Conclusions

Peripheral artery disease (PAD) is an inflammatory disease primarily caused by atherosclerosis, which gradually narrows the arterial lumen. Revascularization is considered the first line therapy for symptomatic obstructive PAD [10, 36]. Catheter-based percutaneous interventions

are an enduring relief for arterial obstruction [36] and are considered the primary method for revascularization [36–38]. Restenosis is defined by a reduction in the diameter of the vessel lumen after angioplasty [39]. Much research and commercialization effort has been devoted to manufacturing device technologies targeting restenosis [40]. The use of polymeric or metallic stents provides better acute results, but these improvements arise at the expense of increased vessel injury [36, 41, 42], with stents commonly resulting in increased risks of thrombosis and stent fracture [43, 44]. The need to address the associated risk that comes with stenting led to non-stent-based local drug delivery. Drug-coated balloons are alternative approaches in which the balloon is coated with a thin, active substance surface layer [36]. Delayed healing along with vascular toxicity of the anti-proliferative agents applied to the balloon's surface was observed in animal studies after DCB angioplasty [36]. In our own prior studies, a nanoparticle delivery system was designed to provide an alternative treatment for PAD, using polyphenols with high therapeutic indices as alternatives to the anti-proliferative agents in commercial products [15]. Similar coatings releasing quercetin and resveratrol from drug eluting stents demonstrated outstanding effects in reducing VSMC proliferation, platelet activation and inflammation, while promoting re-endothelization [45, 46]. The cationic characteristics of the pNP were provided by addition of a cationic Eudragit RL100 polymer during pNP synthesis. By adjusting the amount of positive charge on the system, the pNP were designed to be bio-compatible and biodegradable and proved to meet the specification ideal for cellular uptake and maintaining a continued period of release. The PLGA nanoparticles with pNP(eQ), pNP(eR), as well as quercetin covalently attached to PLGA (pNP(cQ), were developed at a size range of 101 nm. All polyphenols were entrapped separately in PLGA pNPs to allow for their comparison. Similar to prior experiments, entrapped quercetin released rapidly in the first 24 hours except that this time the active substance was entrapped separately in pNPs not together with RESV in its methoxylated form [15]. However, covalent attachment of quercetin delayed its release as indicated by no burst release and a more protracted profile. The methoxylated derivative of quercetin (rhamnazin) with increased hydrophobicity provided a slightly more sustained release of quercetin, although was not as protracted as pNPs possessing covalently-attached Q. In the latter case, release was sustained for a total of 6 days, which is beneficial since vascular healing, as well as the cellular events contributing to restenosis, begin within the first 7 days [47].

In this experiment an ultrasonic coating method was used that allowed our pNP entrapment system to generate a uniform coating. This coating technique will hopefully minimize non-specific release of drug into the blood and enhance the long-term retention of drug within vascular tissue, but such specifications will be addressed in future animal experiments.

In summary, a key parameter for a successful DCB is delivery of therapeutic levels of drug at biologically appropriate time points within a critical time window after endovascular intervention. The synthesized PLGA-based pNP system proved to be biocompatible with a size range required for endocytosis and provided an extended period of release. Importantly, brief application with pNPs containing covalently-attached Q demonstrated an ability to reduce VSMC proliferation at least through 72 hours. Studies utilizing a balloon angioplasty model in small animals aimed at testing the pharmacokinetics of drug delivery to the vascular wall will be required for further development.

Supporting information

S1 Fig. Von Kossa staining of rat aortic smooth muscle cells, demonstrating calcification achieved after two weeks treatment with calcification medium.
(TIF)

Acknowledgments

Author Contributions

Conceptualization: Carlos E. Astete, Dorin Boldor, Cristina M. Sabliov, Tammy R. Dugas.

Data curation: Dorin Boldor, Merilyn H. Jennings, Jake D. Gorman, Tammy R. Dugas.

Formal analysis: Merilyn H. Jennings, Jake D. Gorman, Tammy R. Dugas.

Funding acquisition: Tammy R. Dugas.

Investigation: Ioana Craciun, Carlos E. Astete, Dorin Boldor, Merilyn H. Jennings, Jake D. Gorman, Cristina M. Sabliov.

Methodology: Ioana Craciun, Carlos E. Astete, Dorin Boldor, Merilyn H. Jennings, Cristina M. Sabliov.

Project administration: Carlos E. Astete, Cristina M. Sabliov, Tammy R. Dugas.

Software: Dorin Boldor.

Supervision: Dorin Boldor, Cristina M. Sabliov, Tammy R. Dugas.

Writing – original draft: Ioana Craciun, Tammy R. Dugas.

Writing – review & editing: Carlos E. Astete, Merilyn H. Jennings, Cristina M. Sabliov, Tammy R. Dugas.

References

1. Song P, Rudan D, Zhu Y, Fowkes FJI, Rahimi K, Fowkes FGR, et al. Global, regional, and national prevalence and risk factors for peripheral artery disease in 2015: an updated systematic review and analysis. The Lancet Global Health. 2019; 7(8):e1020–e30. https://doi.org/10.1016/S2214-109X(19)30255-4 PMID: 31303293

2. Patel MR, Conte MS, Cutlip DE, Dib N, Geraghty P, Gray W, et al. Evaluation and treatment of patients with lower extremity peripheral artery disease: Consensus definitions from peripheral academic research consortium (PARC). Journal of the American College of Cardiology. 2015; 65(9):931–41. https://doi.org/10.1016/j.jacc.2014.12.036 PMID: 25744011

3. Jaff MR, Cahill KE, Yu AP, Birnbaum HG, Engelhart Luella MM. Clinical Outcomes and Medical Care Costs Among Medicare Beneficiaries Receiving Therapy for Peripheral Arterial Disease. Annals of Vascular Surgery. 2010; 24(5):577–87. https://doi.org/10.1016/j.avsg.2010.03.015 PMID: 20579582

4. Beckman JA, Findeiss LK, Golzarian J, Gornik HL, Halperin JL, Jaff MR, et al. This article is copublished in Circulation, Catheterization and Cardiovascular Interventions, the Journal of Vascular Surgery, and Vascular Medicine. Jac. 2011; 58(19):2020–45.

5. Fowkes FGR, Aboyans V, Fowkes FJI, McDermott MM, Sampson UKA, Criqui MH. Peripheral artery disease: epidemiology and global perspectives. Nature Reviews Cardiology. 2017; 14(3):156–70. https://doi.org/10.1038/nrcardio.2016.179 PMID: 27853158

6. Marrocco CJ, Bush HRL. Peripheral arterial disease. High Risk Diabetic Foot: Treatment and Prevention. 2010; 358:1–8.

7. Konishi A, Mitsutake Y, Ho M, Handa N, Koike K, Mochizuki S, et al. Patient and lesion characteristics in late/very late stent thrombosis with everolimus-eluting stents from real-world adverse event reporting. Journal of Cardiology. 2019:3–8. https://doi.org/10.1016/j.jjcc.2019.07.016 PMID: 31537439

8. Tendera M, Aboyans V, Bartelink ML, Baumgartner I, Clment D, Collet JP, et al. ESC Guidelines on the diagnosis and treatment of peripheral artery diseases. European Heart Journal. 2011; 32(22):2851–906. https://doi.org/10.1093/eurheartj/ehr211 PMID: 21873417

9. Barrett C, Barshes NR, Corriere MA, Drachman DE, Fleisher LA, Gerry Fowkes FR, et al. 2016 AHA/ACC Guideline on the Management of Patients With Lower Extremity Peripheral Artery Disease. Circulation. 2017; 135:726–79.

10.   Norgren L, Hiatt WR, Dormandy JA, Nehler MR, Harris KA, Fowkes FG, et al. Inter-society consensus for the management of peripheral arterial disease. International angiology: a journal of the International Union of Angiology. 2007; 26(2):81–157.

11.   Urasawa K, Sato K, Koshida R, Honma Y. [Endovascular therapy for peripheral arterial disease]. Nippon rinsho Japanese journal of clinical medicine. 2011; 69(2):318–21. PMID: 21387683

12.   Analysis AE-b. Stenting for peripheral artery disease of the lower extremities: An evidence-based analysis2010. 1–88 p.

13.   Thukkani AK, Kinlay S. Endovascular Intervention for Peripheral Artery Disease. Circulation Research. 2015; 116(9):1599–613. https://doi.org/10.1161/CIRCRESAHA.116.303503 PMID: 25908731

14.   Rogers JH, Laird JR. Overview of new technologies for lower extremity revascularization. Circulation. 2007; 116(18):2072–85. https://doi.org/10.1161/CIRCULATIONAHA.107.715433 PMID: 17967988

15.   Dugas TR, Brewer G, Longwell M, Fradella T, Braun J, Astete CE, et al. Nanoentrapped polyphenol coating for sustained drug release from a balloon catheter. Journal of Biomedical Materials Research—Part B Applied Biomaterials. 2019; 107(3):646–51. https://doi.org/10.1002/jbm.b.34157 PMID: 30091513

16.   Ali RM, Abdul Kader MASK, Wan Ahmad WA, Ong TK, Liew HB, Omar AF, et al. Treatment of Coronary Drug-Eluting Stent Restenosis by a Sirolimus- or Paclitaxel-Coated Balloon. JACC: Cardiovascular Interventions. 2019; 12(6):558–66. https://doi.org/10.1016/j.jcin.2018.11.040 PMID: 30898253

17.   Van Den Berg JC. In-stent restenosis management: The best is yet to come. Journal of Cardiovascular Surgery. 2017; 58(4):508–17. https://doi.org/10.23736/S0021-9509.17.09953-0 PMID: 28322039

18.   Goyal SN, Bharti S, Krishnamurthy B, Agrawal Y, Ojha SK, Arya DS. Impact of metabolic syndrome on re-stenosis development: Role of drug-eluting stents. Diabetes and Vascular Disease Research. 2012; 9(3):177–88. https://doi.org/10.1177/1479164111430336 PMID: 22219135

19.   Werk M, Langner S, Reinkensmeier B, Boettcher HF, Tepe G, Dietz U, et al. Inhibition of restenosis in femoropopliteal arteries. Paclitaxel-coated versus uncoated balloon: Femoral paclitaxel randomized pilot trial. Circulation. 2008; 118(13):1358–65. https://doi.org/10.1161/CIRCULATIONAHA.107.735985 PMID: 18779447

20.   Tepe G, Laird J, Schneider P, Brodmann M, Krishnan P, Micari A, et al. Drug-coated balloon versus standard percutaneous transluminal angioplasty for the treatment of superficial femoral and popliteal peripheral artery disease 12-month results from the IN.PACT SFA randomized Trial. Circulation. 2015; 131(5):495–502. https://doi.org/10.1161/CIRCULATIONAHA.114.011004 PMID: 25472980

21.   Tepe G, Zeller T, Albrecht T, Heller S, Schwarzwälder U, Beregi JP, et al. Local delivery of paclitaxel to inhibit restenosis during angioplasty of the leg. New England Journal of Medicine. 2008; 358(7):689–99. https://doi.org/10.1056/NEJMoa0706356 PMID: 18272892

22.   Cortese B, Granada JF, Scheller B, Schneider PA, Tepe G, Scheinert D, et al. Drug-coated balloon treatment for lower extremity vascular disease intervention: An international positioning document. European Heart Journal. 2016; 37(14):1096–103. https://doi.org/10.1093/eurheartj/ehv204 PMID: 26009594

23.   Doshi M, Sojitra P, Shah D, Dani S, Abizaid A. Technical Insights on Drug-Coated Balloons II. Drug-Coated Balloons. 2019:45–57.

24.   Marzullo R, Aprile A, Clementi F, Stella P, Modena MG, Sangiorgi GM. Paclitaxel eluting balloon: From bench to bedside. Minerva Cardioangiologica. 2009; 57(5):597–609. PMID: 19838150

25.   McFadden EP, Stabile E, Regar E, Cheneau E, Ong ATL, Kinnaird T, et al. Late thrombosis in drug-eluting coronary stents after discontinuation of antiplatelet therapy. Lancet. 2004; 364(9444):1519–21. https://doi.org/10.1016/S0140-6736(04)17275-9 PMID: 15500897

26.   Farb A, Heller PF, Shroff S, Cheng L, Kolodgie FD, Carter AJ, et al. Pathological analysis of local delivery of paclitaxel via a polymer-coated stent. Circulation. 2001; 104(4):473–9. https://doi.org/10.1161/hc3001.092037 PMID: 11468212

27.   Fda. August 7, 2019 UPDATE: Treatment of Peripheral Arterial Disease with Paclitaxel-Coated Balloons and Paclitaxel-Eluting Stents Potentially Associated with Increased Mortality. 2019; 57:13–5.

28.   Yurdagul A, Kleinedler JJ, McInnis MC, Khandelwal AR, Spence AL, Orr AW, et al. Resveratrol promotes endothelial cell wound healing under laminar shear stress through an estrogen receptor-α-dependent pathway. American Journal of Physiology—Heart and Circulatory Physiology. 2014; 306(6):797–806. https://doi.org/10.1152/ajpheart.00892.2013 PMID: 24464753

29.   Narula N, Olin JW, Narula N. Pathologic disparities between peripheral artery disease and coronary artery disease. Arteriosclerosis, thrombosis, and vascular biology. 2020; 40(9):1982–9. https://doi.org/10.1161/ATVBAHA.119.312864 PMID: 32673526

30.   Karwowski W, Naumnik B, Szczepański M, Myśliwiec M. The mechanism of vascular calcification–a systematic review. Medical science monitor: international medical journal of experimental and clinical research. 2012; 18(1):RA1.

31. Fitzgerald PJ, Ports TA, Yock P. Contribution of localized calcium deposits to dissection after angioplasty. An observational study using intravascular ultrasound. Circulation. 1992; 86(1):64–70. https://doi.org/10.1161/01.cir.86.1.64 PMID: 1617791

32. Fanelli F, Cannavale A, Gazzetti M, Lucatelli P, Wlderk A, Cirelli C, et al. Calcium burden assessment and impact on drug-eluting balloons in peripheral arterial disease. Cardiovascular and interventional radiology. 2014; 37(4):898–907. https://doi.org/10.1007/s00270-014-0904-3 PMID: 24806955

33. Trion A, van der Laarse A. Vascular smooth muscle cells and calcification in atherosclerosis. American heart journal. 2004; 147(5):808–14. https://doi.org/10.1016/j.ahj.2003.10.047 PMID: 15131535

34. Preibisch S, Saalfeld S, Tomancak P. Globally optimal stitching of tiled 3D microscopic image acquisitions. Bioinformatics. 2009; 25(11):1463–5. https://doi.org/10.1093/bioinformatics/btp184 PMID: 19346324

35. Harding IS, Rashid N, Hing KA. Surface charge and the effect of excess calcium ions on the hydroxyapatite surface. Biomaterials. 2005; 26(34):6818–26. https://doi.org/10.1016/j.biomaterials.2005.04.060 PMID: 15955555

36. Byrne RA, Joner M, Alfonso F, Kastrati A. Drug-coated balloon therapy in coronary and peripheral artery disease. 2013.

37. Wiseman JT, Fernandes-Taylor S, Saha S, Havlena J, Rathouz PJ, Smith MA, et al. Endovascular Versus Open Revascularization for Peripheral Arterial Disease. Ann Surg. 2017; 265(2):424–30. https://doi.org/10.1097/SLA.0000000000001676 PMID: 28059972

38. AbuRahma AF. When Are Endovascular and Open Bypass Treatments Preferred for Femoropopliteal Occlusive Disease? Annals of Vascular Diseases. 2018;advpub. https://doi.org/10.3400/avd.ra.18-00001 PMID: 29682105

39. Omeh DJ, Shlofmitz E. Restenosis. StatPearls [Internet]. 2020.

40. Curcio A, Torella D, Cuda G, Coppola C, Faniello MC, Achille F, et al. Effect of stent coating alone on in vitro vascular smooth muscle cell proliferation and apoptosis. American Journal of Physiology-Heart and Circulatory Physiology. 2004; 286(3):H902–H8. https://doi.org/10.1152/ajpheart.00130.2003 PMID: 14592937

41. Kuntz RE, Baim DS. Defining coronary restenosis. Newer clinical and angiographic paradigms. Circulation. 1993; 88(3):1310–23. https://doi.org/10.1161/01.cir.88.3.1310 PMID: 8353892

42. Costa MA, Simon DI. Molecular basis of restenosis and drug-eluting stents. Circulation. 2005; 111 (17):2257–73. https://doi.org/10.1161/01.CIR.0000163587.36485.A7 PMID: 15867193

43. Rocha-Singh KJ, Bosiers M, Schultz G, Jaff MR, Mehta M, Matsumura JS, et al. A single stent strategy in patients with lifestyle limiting claudication: 3-year results from the Durability II trial. Catheterization and Cardiovascular Interventions. 2015; 86(1):164–70. https://doi.org/10.1002/ccd.25895 PMID: 25676568

44. Scheinert D, Scheinert S, Sax J, Piorkowski C, Bräunlich S, Ulrich M, et al. Prevalence and clinical impact of stent fractures after femoropopliteal stenting. Journal of the American College of Cardiology. 2005; 45(2):312–5. https://doi.org/10.1016/j.jacc.2004.11.026 PMID: 15653033

45. Kleinedler JJ, Foley JD, Orchard EA, Dugas TR. Novel nanocomposite stent coating releasing resveratrol and quercetin reduces neointimal hyperplasia and promotes re-endothelialization. Journal of Controlled Release. 2012; 159(1):27–33. https://doi.org/10.1016/j.jconrel.2012.01.008 PMID: 22269665

46. Kleinedler JJ, Foley JD, Alexander JS, Roerig SC, Hebert VY, Dugas TR. Synergistic effect of resveratrol and quercetin released from drug-eluting polymer coatings for endovascular devices. Journal of Biomedical Materials Research Part B: Applied Biomaterials. 2011; 99(2):266–75. https://doi.org/10.1002/jbm.b.31894 PMID: 21948767

47. Kenagy RD. 7• Biology of Restenosis and Targets for Intervention. Mechanisms of Vascular. 2011: 115.